Ballistic Range Tests of Ablating and Nonablating Slender Cones

PETER F. INTRIERI,* DONN B. KIRK,* GARY T. CHAPMAN,† AND JAMES E. TERRY‡
NASA Ames Research Center, Moffett Field, Calif.

The feasibility of using a ballistic range to study effects of ablation on the aerodynamic characteristics of slender cones is discussed. Calculations indicate that with the proper choice of test conditions, models made of realistic heat-shield type materials can achieve near steady-state ablation over their entire conical surface early in the flight. A series of ballistic range tests of ablating and nonablating 10° cones is described and experimental data consisting of drag, static and dynamic stability, and lift are presented. The experimental data show that ablation significantly reduces the drag and static stability but has little effect on dynamic stability and lift. Calculations show that the measured reduction in drag coefficient can be attributed to the loss in skin friction due to ablation, but that this loss in skin friction accounts for only about one third of the measured reduction in static stability. Similar conclusions are obtained when the same calculations are applied to wind-tunnel ablation data (paradichlorobenzene models). Finally, it is shown that the angular motions of the ablating models are markedly different from and less regular than those of the nonablating models.

Nomenclature

A = reference area (model base area)
C_D = drag coefficient
$C_{L\alpha}$ = lift-curve slope
C_{Lo}, C_{yo} = lift and side force coefficients at zero angle of attack
C_{m_α} = quasi-linear pitching-moment curve slope
$C_{m_{\alpha f}}$ = pitching-moment curve slope due to longitudinal skin friction
$C_{m_q} + C_{m_{\dot\alpha}}$ = damping-in-pitch derivative, $\partial C_m/\partial(qd/V) + \partial C_m/\partial(\dot\alpha d/V)$
c = specific heat
d = reference length (model base diameter)
I_Y = moment of inertia about a transverse axis through the center of gravity
K = thermal conductivity
L = latent heat of vaporization
l = model length
M = Mach number
m = model mass
$\dot m$ = total mass loss rate
$\dot m/\rho VA$ = ablation parameter (steady state)
p = roll rate about axis of symmetry of model
q = angular pitching velocity
Re = Reynolds number based on freestream conditions and model length
r_b = model base radius
r_n = nose radius
T_a = $T_{\text{abl}} - T_i$
T_{abl} = ablation temperature
T_i = initial temperature
T_{melt} = melting temperature
t = time
V = freestream velocity
x = distance flown
x_{cg} = axial distance from model nose to center of gravity
y = horizontal coordinate normal to the flight path
z = coordinate normal to the flight path and y axis
α = angle of attack (in the vertical plane)
α^* = transpiration effectiveness parameter for laminar boundary layer
β = angle of sideslip (in the horizontal plane)
ζ = $cT_a + L$
η_1, η_2 = damping exponents in Eq. (3)
θ = angular displacement measured in the xz plane
λ = wavelength of pitching oscillation
ξ = dynamic stability parameter for unpowered flight at constant altitude
ρ = freestream air density
ρ_o = earth sea-level density
ρ_m = material density
σ = resultant angle of attack, $\tan^{-1}(\tan^2\alpha + \tan^2\beta)^{1/2}$
$\bar\sigma_m$ = average maximum resultant angle of attack
σ_{rms} = root-mean-square resultant angle of attack, $\left(\frac{1}{x}\int_0^x \sigma^2 dx\right)^{1/2}$
ψ = angular displacement measured in the xy plane
ω_1, ω_2 = rates of rotation of vectors that describe the model oscillatory motion in Eq. (3)
$\omega d/V$ = reduced frequency parameter

Presented as Paper at the AIAA 7th Aerospace Sciences Meeting, New York, January 20–22, 1969; submitted February 13, 1969; revision received August 18, 1969.

* Research Scientist.
† Research Scientist. Member AIAA.
‡ Research Scientist; now Engineer, Aero Commander, Bethany, Okla. Member AIAA.

Introduction

IT has been recognized for several years that ablation of the heat shield could significantly affect the aerodynamic characteristics of slender cones. A number of experimental studies have been conducted in various wind tunnels to investigate this phenomenon. However, since the heating environment available in most wind tunnels is not sufficiently severe to attain ablation of actual heat-shield materials, the ablation process has been simulated either by injecting gas through a porous skin of a model or by coating the model with a low-temperature subliming material. These two simulation techniques have not, for the most part, led to the same conclusions. This is due both to actual differences between the two processes, and to failure in identifying and matching all important parameters.

The first such investigation was conducted by Syvertson and McDevitt,[1,2] who injected gas uniformly through the skin of a slender porous cone. They found decreases in both normal force and pitching moment that became more pronounced as they increased the mass injection. This significant result caused others to attempt a closer look at actual ablation. Chrusciel and Chang[3] coated slender conical models with subliming materials (paradichlorobenzene and ammonium chloride) and tested the configurations in a wind tunnel. For their range of conditions, normal force was unaffected, but the moment curve slope decreased. Many other investigations along these lines have been made (see, for

example, Refs. 4–17). All have been in wind tunnels and most have used either mass injection or materials that readily ablate.

Ballistic range tests could offer some important advantages in determining the aerodynamic characteristics of ablating bodies. First, they could provide a good approximation of the aerothermodynamic environment of ablating entry vehicles. Models made of realistic heat-shield-type materials would undergo ablation in very nearly the same way as in full-scale flight; e.g., for a laminar boundary layer the imposed heating rate and hence the local mass loss rate vary inversely with the square root of distance from the nose. Secondly, with the models in free flight, the aerodynamic coefficients could be studied without support interference effects. And thirdly, there would be complete freedom for effects of model oscillation on the ablation processes to act.

The feasibility of using a ballistic range to study the effects of ablation has been considered in Ref. 18. The theoretical study presented therein shows that, by a proper choice of test conditions and model material, near steady-state ablation rates can be achieved over the entire conical surface of a model early in its flight. In the present paper, the experimental aerodynamic characteristics obtained from ballistic range tests of both ablating and nonablating slender cones are presented.

Predicted Test Conditions for Ablation

In the design of a ballistic range test of an ablating body, the following factors must be considered. 1) The ablation parameter ($\dot{m}/\rho VA$) should be within the range where other investigations indicate an effect of ablation on aerodynamic characteristics in order that meaningful comparisons may be made. This parameter is the ratio of the mass loss rate of ablation products to the freestream mass flow through area A (model base area). 2) Near steady-state ablation over the entire model surface should be achieved early in the flight. 3) The geometry of the configuration should not change significantly during the flight.

Each of these factors has been considered for cones, and the methods of calculation, which assume a subliming ablator, are described in Ref. 18. The calculations were performed for the plastics Delrin, Teflon, and Lexan. These materials were chosen because they are representative of realistic heat-shield-type materials, and they are sufficiently strong to be considered for gun launching in a ballistic range. The most reliable material properties the authors were able to determine for these three materials are listed in Table 1.

The results of these calculations for a Delrin model (10° half-angle cone, 2.54 cm long) after 15 m of flight are shown in Fig. 1. In this figure, model velocity is plotted versus the ratio of freestream density to earth sea level density, and lines of constant $\dot{m}/\rho VA$ and percent of steady-state ablation achieved at the most aft point on the cone are shown. A curve showing constant Reynolds number conditions is also indicated. To give an example of what is shown here, consider tests at a velocity of 6 km/sec at a density ratio of 0.2.

Table 1 Material properties

Property	Delrin		Teflon		Lexan	
c, cal/g °K	0.306	Ref. 27	0.3	Ref. 30	0.3	Ref. 29
K, cal/sec cm °K	6.62×10^{-4}	Ref. 29	5.79×10^{-4}	Ref. 29	4.55×10^{-4}	Ref. 29
L, cal/g	789	Ref. 27	382	Ref. 30	1110	Ref. 28
T_{abl}, °K	493	Ref. 27	760	Ref. 30	554	[b]
T_i, °K	293	[c]	293	[c]	293	[c]
T_{melt}, °K	445	Ref. 27	Sublimes		528	Ref. 29
α^* ND	0.34	Ref. 28	0.26	Ref. 19	0.40	Ref. 28
ζ, cal/g	850	Ref. 27	522	Ref. 30	1190	Ref. 28
ρ_m, g/cm³	1.43	[a]	2.15	Ref. 29	1.20	[a]

[a] Value measured by authors.
[b] 5% above T_{melt} (assumed).
[c] Assumed value.

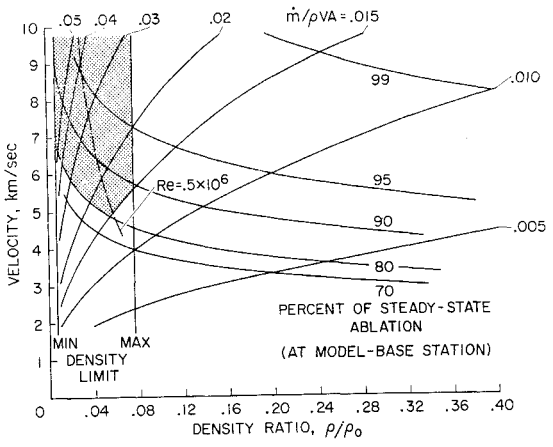

Fig. 1 Test conditions for ablation of a 10° Delrin cone; $l = 2.54$ cm, $x = 15$ m.

If the model flew at these test conditions for infinite time, it would achieve an ablation rate, $\dot{m}/\rho VA$, of 0.01. However, it is seen that after only 15 m of flight it has achieved approximately 95% of this steady-state ablation rate.

Somewhat arbitrary decisions must now be made concerning the minimum ablation rate that would yield meaningful results. Other investigations have indicated that values of $\dot{m}/\rho VA$ of about 0.01 or greater can significantly affect the aerodynamic characteristics of slender cones. Therefore, for useful ballistic range tests a value of $\dot{m}/\rho VA$ of about this magnitude should be achieved early in the trajectory and should not change greatly during the remainder of the flight. With this in mind, it was stipulated that the steady-state value of $\dot{m}/\rho VA$ must exceed 0.015; furthermore, the local mass loss rate at the model base station must exceed 80% of its steady-state value within the first 15 m of flight. Thus the value of $\dot{m}/\rho VA$ actually attained is above 0.012 from 15 m to the end of the range.

In order to obtain valid aerodynamic coefficients there should be at least $1\frac{1}{2}$ cycles of model motion observed. However, the frequency of oscillation should not be so high that the motion is poorly defined. These two factors, in combination with the number of data stations in the particular range to be used and the particular model design chosen, determine the minimum and maximum freestream density for the tests. The shaded region in Fig. 1 gives the test boundaries determined in this manner for the Ames Pressurized Ballistic Range. Under these criteria, it is noted that velocities greater than 4.9 km/sec are necessary to achieve the desired results.

The test region shown in Fig. 1 also has an upper bound dictated by too large a change in the model geometry. However, calculations of both nose and surface recession indicated that this is not a significant consideration within the shaded region.

It was also shown[18] that, of the three materials considered (Teflon, Delrin, and Lexan), it is advantageous to use Delrin as the model material since it achieves a given ablation rate at the lowest velocity. The desirable testing regime (with boundaries as defined previously) for each of these materials is compared in Fig. 2 and the decided advantage in testing Delrin models is obvious.

Ballistic Range Tests

Facility

The tests were performed by launching models from a gun into the Ames Pressurized Ballistic Range. This facility is a cylindrical tank about 3 m in diameter which can be pressurized or evacuated. There are 24 orthogonal spark shadowgraph stations irregularly spaced over the 62-m length of the

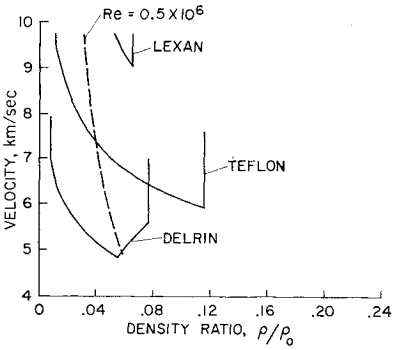

Fig. 2 Effect of model material on test conditions for ablation; 10° cone, l = 2.54 cm, x = 15 m.

facility, providing shadowgraph pictures from which x, y, z, θ, and ψ coordinates were read (the roll angle, and hence roll rate, could not be measured for these tests). The linear coordinates were measured to within 0.007 cm, and the angles to within 0.5°. The orientation angles θ and ψ were read relative to earth fixed axes. Corrections were made for the angle between the resultant model velocity and the earth fixed axes to give values of α and β. Time of model flight between stations was recorded with electronic chronographs accurate to within $\frac{5}{8}$ μsec.

The tests described here are the highest speed tests (5.6 km/sec) ever made in this particular facility. For most configurations at these speeds, radiation from the model shock layer and wake is intense enough to completely fog the photographic film. However, for the slender cones being considered, this was not a serious problem, but a sabot stripper was required to prevent the sabot fingers from entering the range and badly fogging the film.

Gun

The models were launched from a deformable-piston light-gas gun[19] having a bore diameter of 1.27 cm. Successful launches were made at muzzle velocities between 5.0 and 5.6 km/sec into still air at a density ratio of 0.04. This is within the desired testing region shown in Fig. 1, i.e., $\dot{m}/\rho VA \approx 0.02$ and percent of steady-state ablation (at the model base station) $\approx 80\%$. Because of the fairly heavy weights being launched (model + sabot + pusher $\approx$ 5 g), the gun was operated near its maximum capability.

Models and Sabots

Sketches of the models and sabots used in the present tests are shown in Fig. 3. The models were 10° half-angle cones and were hollowed out at the base to make them aerodynamically stable. For the ablation tests, the models were made of Delrin. Because these models were so fragile, it was necessary to fully encapsulate them with the sabot fingers and to fill the void in the model base, during launch, with a plug. The four sabot fingers were made of Lexan because it is both stronger and lighter than Delrin, although it radiates more intensely in high-speed flight. Successful flights were also made with nonablating metal models at the same conditions as the ablation tests (i.e., V $\approx$ 5 km/sec, $\rho/\rho_0 \approx 0.04$). Since it was known from previous experience that aluminum burned at these conditions, the noses of these models were made of tantalum, which prevented significant nose blunting. The tantalum tips were 0.20l long and were threaded into aluminum aftersections. These models had the same center of gravity location as the Delrin models.

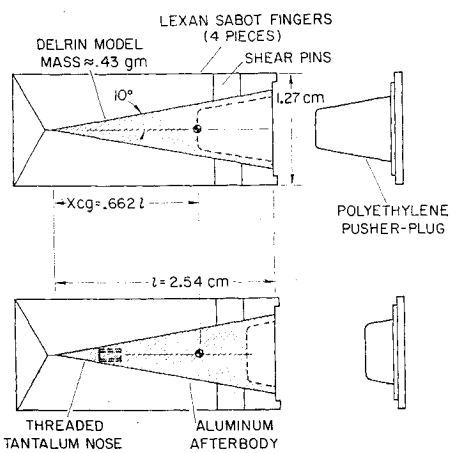

Fig. 3 Sketches of models and sabots.

Typical shadowgraphs of both an ablating and a nonablating model at the last observation station (no. 24) after 67 m of flight are presented in Figs. 4a and 4b, respectively. These shadowgraphs are not as clear as would be obtained at lower velocities where the facility shadowgraph system was designed to operate. Because of the high velocities, it can be seen that the images of the models are somewhat blurred; also, the low contrast evident in these pictures is due to some fogging of the film from model and flowfield radiation. The pictures show that the flow over both the ablating and nonablating models is laminar well into the wake; the wake remained laminar for the entire length observed in the original shadowgraphs (about 16 model lengths). It can also be seen in Fig. 4 that as a result of the mass addition into the boundary layer, due to ablation, the diameter of the wake of the ablating model is significantly greater than that of the nonablating model, by about 35% at a distance of 5 model lengths behind the model base. Careful measurements made from many of the best shadowgraphs obtained (similar to those presented in Fig. 4) indicated no large or systematic thickening of the flowfield around the model due to ablation. At a given resultant angle of attack and with comparable values of r_n/r_b, any difference in the angle and/or standoff distance of the bow shock wave between the ablating and nonablating models was less than the reading accuracy. The shock wave angle shown in Fig. 4a is greater than that in Fig. 4b due to the larger resultant angle of attack. It should also be noted in Fig. 4 that the amount of nose blunting obtained during flight is tolerable and approximately the same in both cases (the maximum nose bluntness, r_n/r_b, obtained at the end of the flights was in the range of 0.04 to 0.07).

Reduction of Data

The data reduction techniques used to deduce the aerodynamic coefficients of drag, lift, and static and dynamic

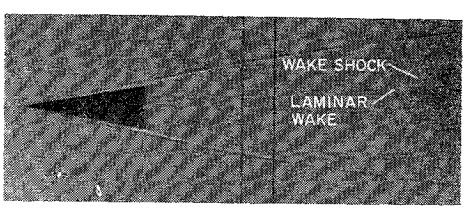

a) Ablating Delrin model; α = 0.77° (β = 5.65°)

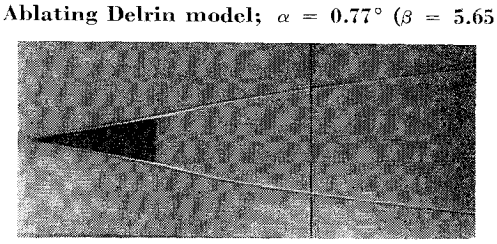

b) Nonablating metal model; α = 0.46° (β = 1.32°)

Fig. 4 Shadowgraphs of models; $V \approx 5$ km/sec, $\rho/\rho_0 = 0.04$, x = 67 m.

stability from free-flight data at the Hypersonic Free-Flight Branch of the Ames Research Center are presented in Ref. 20. In this section it will be necessary to present only the basic equations used and a brief description of these techniques.

Drag

Drag coefficients were obtained directly from the flight time and distance measurements by the method presented in Ref. 20, which assumes a constant drag coefficient. The equation relating time and distance can be written[21]

$$t = t_o - (1/V_o k C_D) + (e^{kC_D x}/V_o k C_D) \quad (1)$$

where V_o and t_o are velocity and time at $x = 0$ and $k = \rho A/2m$. The parameters C_D, V_o, and t_o are determined which give the "best fit" to the measured values of x and t. A method applicable to cases where the drag coefficient varies with angle of attack is presented in Ref. 22. It is shown therein that if the drag coefficient varies with the resultant angle of attack according to the relation

$$C_D = C_{D_o} + C_{D_2}\sigma^2 \quad (2)$$

then the effective drag coefficient obtained from Eq. (1) is the drag coefficient that would be obtained at a constant angle of attack equal to the root-mean-square resultant angle of attack of a given flight. The present results were found to be represented adequately by Eq. (2), as will be shown.

Static and Dynamic Stability Derivatives

The stability derivatives were determined from analysis of the pitching and yawing motions experienced by the models during free flight. The analysis consisted in fitting the following well known tricyclic equation, derived by Nicolaides,[23] to the measurements of α and β of each flight:

$$\beta + i\alpha = K_1 e^{(\eta_1 + i\omega_1)x} + K_2 e^{(\eta_2 - i\omega_2)x} + K_3 e^{ipx} \quad (3)$$

where $\eta_{1,2}$ and $\omega_{1,2}$ are functions of the aerodynamic stability coefficients and $K_{1,2,3}$ are functions of the initial conditions. The most important assumptions inherent in this equation are linear aerodynamics, small angles of attack, constant roll rate, and small asymmetries. In the present analysis it was further assumed that the Magnus moment was zero. A least squares procedure using differential corrections was used to determine optimum values of the constants.

The static and dynamic stability parameters are related to the constants in Eq. (3) as follows. The wavelength of the oscillation is given by

$$\lambda = 2\pi/(\omega_1\omega_2)^{1/2} \quad (4)$$

The quasi-linear pitching-moment curve slope, C_{m_α}, is computed from the relation

$$C_{m_\alpha} = -8\pi^2 I_y/\lambda^2 \rho A d \quad (5)$$

The dynamic stability parameter, ξ, defined as

$$\xi = C_D - C_{L_\alpha} + (md^2/I_y)(C_{m_q} + C_{m_{\dot\alpha}}) \quad (6)$$

is determined from the constants η_1 and η_2 by means of the relation

$$\xi = (\eta_1 + \eta_2)/(\rho A/2m) \quad (7)$$

It has been shown[24,25] that ξ is a measure of the dynamic stability of a vehicle both in unpowered flight at constant altitude and in ballistic entry.

Lift

An effective lift-curve slope, C_{L_α}, was obtained for each flight by analyzing the swerving motion of the model, in conjunction with the oscillatory motion of the model given by Eq. (3). A modified form of Nicolaides' equation[23] is fitted by the method of least squares to the measured displacement data y and z. The equation used is

$$y + iz = -\frac{\rho A}{2m}\left\{C_{L_\alpha}\int_0^x\int_0^x (\beta + i\alpha)dxdx + (C_{y_o} + iC_{L_o}) \times \left(\frac{1 + ipx - e^{ipx}}{p^2}\right)\right\} + (y'_o + iz'_o)x + (y_o + iz_o) \quad (8)$$

The constants C_{y_o} and C_{L_o} are necessary to account for small model asymmetries. For a body of revolution they should be identically zero.

	THEORY		EXPERIMENT	
	NO ABLATION	ABLATION	NO ABLATION	ABLATION
WAVE DRAG (KOPAL)	0.065	SAME		
SKIN FRICTION	.039	0.010		
BASE DRAG	.007	SAME		
VISCOUS INTERACTION	.004	.006		
TOTAL DRAG (α=0°)	0.115	0.088	0.112	0.086

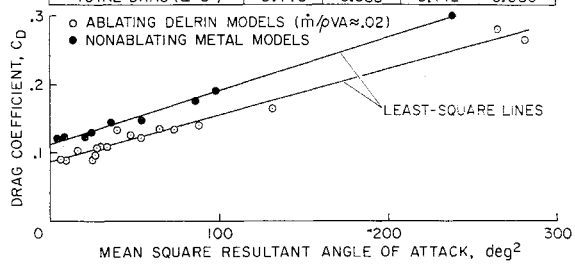

Fig. 5 Drag data, $M \approx 15$, $Re \approx 0.4 \times 10^6$.

Experimental Results

Drag Characteristics

Experimental data were obtained at a nominal Mach number of 15 and a nominal Reynolds number based on model length of 0.4 million. As stated previously, at these test conditions the flow over the model was laminar. In Fig. 5, the experimental values of drag coefficient are plotted versus the mean-square resultant angle of attack $(\sigma_{\text{rms}})^2$ and it can be seen that straight lines correlate the data, consistent with Eq. (2). Comparison of the data from the ablating and nonablating models shows that for the angle-of-attack range investigated, ablation reduced the drag coefficient by about 0.03, approximately 25% at $\alpha = 0°$. Calculated components of the drag coefficient shown in this figure (i.e., wave drag, skin friction, base drag, viscous interaction) were made for $\alpha = 0°$ assuming both zero ablation and steady-state ablation. The required heat-transfer and skin-friction calculations depended heavily on the boundary-layer program described in Ref. 26 modified to include blowing at the wall. The important thing to note in Fig. 5 is that the calculated drag coefficient assuming zero ablation was 0.115, while that assuming steady-state ablation was 0.088. These values are seen to be in excellent agreement with those obtained by extrapolation of the experimental data to $\alpha = 0°$. The difference in drag coefficient between the ablating and nonablating models is primarily attributable to the large reduction in skin friction (about 75%) due to ablation. Since the calculation assuming steady-state ablation is nearly identical with the experimental result, it seems likely that the test conditions did result in a high fraction of steady-state ablation, as predicted in Fig. 1.§ Another factor tending to substantiate the ablation rate calculations is that no significant difference in drag coefficient could be detected between the earliest portion and the final portion of the observed trajec-

§ Because of the high heating rates and relatively low model surface pressure (approximately one-third of an atmosphere), it is probable that sublimation accounted for most of the mass removal in the present tests.

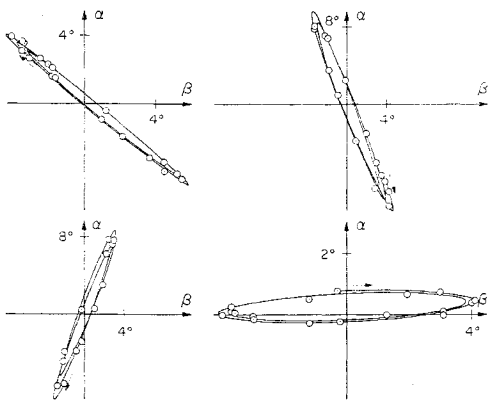

a) Nonablating models

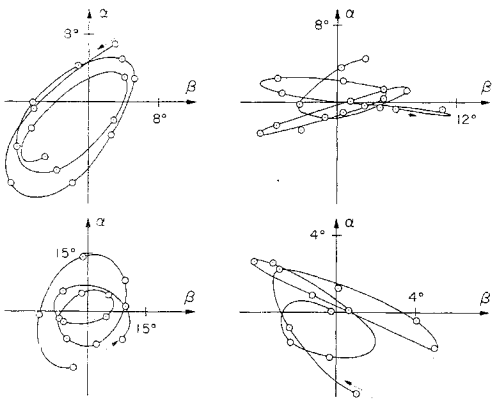

b) Ablating models

Fig. 6 Typical angular motions of models.

tory; i.e., near steady-state ablation was achieved early in the flight; hence no significant increase occurred with distance flown. The percent of steady-state ablation rate achieved at the model base station was estimated[18] to be about 80% after 15 m of flight and about 90% at the end of the flight (67 m), an increase of only about 10%.

Model Motions

As previously discussed, lift and stability coefficients are obtained from analysis of the oscillatory and swerving motions of models in free flight. One of the most interesting results of the present tests was the model motions themselves. This is illustrated in Fig. 6, which shows some of the angular orientation histories for both nonablating and ablating models. In this figure the angle of attack, α, is plotted versus the angle of sideslip, β; the circles show the measured data and the lines are hand fairings of these data. It can be seen that about $2\frac{1}{2}$ cycles of model motion were obtained for each flight of both the nonablating and ablating models and that about 7 or 8 values of α and β per cycle were obtained to define the motion. This number of cycles and data points per cycle are usually sufficient to obtain reliable aerodynamic coefficients.

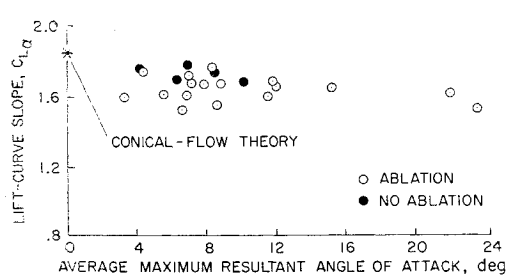

Fig. 7 Lift data, $M \approx 15$, $Re \approx 0.4 \times 10^6$.

As indicated in Fig. 6a, all the motions obtained for the nonablating models were similar in appearance. The motions are seen to be nearly planar with little roll, a type of motion frequently obtained in ballistic ranges. Conversely, some of the motions obtained for the ablating models (Fig. 6b) were very irregular. For these motions the character of each cycle is not repeated and the excursions seem almost random. The reasons for the marked effect of ablation on some of the motions are not known. It is conceivable that such factors as small imperfections in the plastic or unsymmetrical tip blunting could, when coupled with ablation, produce variable roll rates, trim angles, etc. which would affect the motions. These effects would probably be more pronounced for small models.

Theoretical motions are obtained by fitting Eq. (3) to the experimental α,β data. The closeness of the theoretical motions to the experimental data is a measure of the reliability of both the lift and stability results. The fitted curves for all the flights of nonablating models and most of the flights of ablating models analyzed in this investigation gave a standard deviation that was within the stated measuring accuracy. However, Eq. (3) could not provide a fit to the experimental data of several flights of ablating models (instead of converging, the solution diverged). Hence, no experimental aerodynamic coefficients could be deduced from these flights. It is believed that ablation so highly influenced these motions that Eq. (3) was not applicable.

Lift Characteristics

The experimental values of the lift-curve slope, $C_{L\alpha}$, are plotted in Fig. 7 vs the average maximum resultant angle of attack. Comparison of the data with and without ablation shows that ablation has only a small effect on lift. The nonablation data show that $C_{L\alpha}$ decreases slightly with increasing angle of attack, and that the value of C_{L_α} obtained by extrapolation of these experimental data to $\alpha = 0°$ is in good agreement with the value predicted by conical flow theory. Since the experimental values of $C_{L\alpha}$ are plotted versus an average angle of attack, comparison of these data with values obtained from theory is not justified at angles of attack other than zero; however, it should be noted that Newtonian theory predicts a similar nonlinear variation of $C_{L\alpha}$ with angle of attack. The data in Fig. 7 show that the ablating cones developed about 5% less lift, for the most part, than the nonablating cones. The ablation data also appear to be more linear within the angle-of-attack range covered. It is noted in this figure that the ablation data show relatively large scatter. This might be expected considering some of the uncommon motions (Fig. 6b) obtained for the ablating models.

Dynamic Stability Characteristics

The experimental values of the dynamic-stability parameter, ξ, as defined by Eq. (6), are plotted in Fig. 8 vs the average maximum resultant angle of attack. These data show that at the present test conditions both the nonablating and

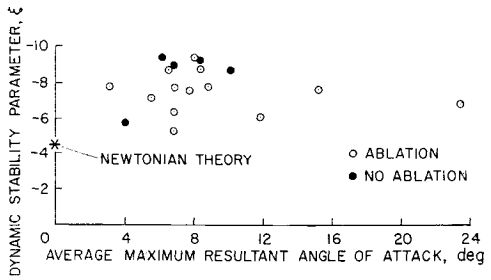

Fig. 8 Dynamic stability data (ξ); $M \approx 15$, $Re \approx 0.4 \times 10^6$, $x_{cg}/l = 0.662$, $\omega d/V \approx 0.003$.

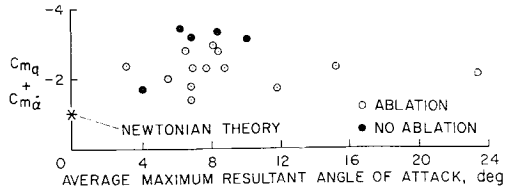

Fig. 9 Dynamic stability data ($Cm_q + Cm_{\dot\alpha}$); $M \approx 15$ $Re \approx 0.4 \times 10^6$, $x_{cg}/l = 0.662$, $\omega d/V \approx 0.003$.

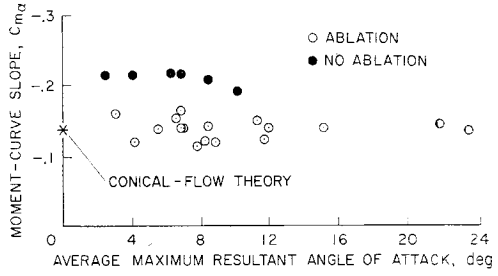

Fig. 10 Static stability data; $M \approx 15$, $Re \approx 0.4 \times 10^6$, $x_{cg}/l = 0.662$.

ablating models are dynamically stable and that ablation has no major effect on the dynamic stability; for most of the angle-of-attack range covered, ablation appears to reduce the dynamic stability a moderate amount.¶ It should be noted here that a value of ξ of -10 is equivalent to a convergence of about 15% per cycle for the present test conditions. The data in Fig. 8 also show that Newtonian theory predicts less dynamic stability than is actually obtained. Careful examination of the data suggest the following additional observations.

1) The dynamic stability data obtained for the nonablating models at angles of attack above 6° show little scatter. An error analysis of these data showed that the scatter in ξ should be about ± 0.5, approximately the scatter obtained. It is indicated, therefore, that although only one value of ξ was obtained below a $\bar\sigma_m$ of 6°, the dynamic stability of the nonablating models is reduced in this low-angle-of-attack range. This is in qualitative agreement with the experimental results presented in Ref. 5.

2) The error analysis for the ablation data showed that the scatter should be less than that for the nonablation data; it can be seen, however, that this scatter is relatively large. It is indicated then that this scatter is real and probably due to varying effects of ablation from flight to flight and possibly within each flight. These varying effects of ablation could be caused by differences in model roll rate, initial orientation, and initial tip geometry, among other things.

3) Finally, within the scatter it appears that the dynamic stability of the ablating models is essentially independent of angle of attack for the angle-of-attack range covered by the present tests.

The experimental values of the damping-in-pitch derivative ($C_{m_q} + C_{m_{\dot\alpha}}$), calculated using Eq. (6), are presented in Fig. 9. The experimental values of ξ, C_D, and C_{L_α} obtained in the present tests were used to perform the calculations. These data lead to the same conclusions as those stated in relation to Fig. 8.

Static Stability Characteristics

The experimental values of the pitching-moment curve slope, C_{m_α}, are plotted in Fig. 10 vs the average maximum resultant angle of attack. Comparison of the data with and without ablation shows that ablation reduces the static stability appreciably, by about 35%. Since the experimental data presented in Fig. 7 showed little effect of ablation on lift, the difference in static stability must be due to a difference in center-of-pressure location between the ablating and nonablating models. It is most interesting, however, to note in Fig. 10 that the static stability of the ablating models is in good agreement with that predicted by conical flow theory (also Newtonian theory) at zero angle of attack, and that the static stability of the nonablating models is greater than that predicted by theory by about 50%.** This important result is strong experimental evidence that a sizable moment producing mechanism(s) which is not adequately accounted for in conical flow or Newtonian theory is present in the nonablation data; furthermore, this mechanism is either removed or its effect on static stability is greatly diminished when the model surface ablates. One such mechanism is skin friction.

A relatively simple estimate of the moment contribution due to longitudinal skin friction was made by calculating the skin friction on the top and bottom rays of a cone at a small angle of attack. A cosine variation was assumed between these rays and the skin-friction results of Ref. 26 were used in the calculations. The results of these calculations for a 10° half-angle cone at $M = 15$, $Re = 0.4 \times 10^6$, and a wall temperature of 300°K showed that the restoring moment due to longitudinal skin friction, $C_{m_{\alpha f}}$, was about -0.025 (statically stabilizing). It can be seen by comparison with the data presented in Fig. 10 that this constitutes only about one-third of the difference between the experimental nonablation data and conical flow theory.†† The remainder might be accounted for by the crossflow skin-friction effects that would also diminish with ablation; however, these calculations must account for the complete three-dimensionality of the flow and have not been performed. Further research is warranted in this area.

It should be noted in relation to Fig. 10 that the large percentage difference in C_{m_α} between the nonablation data and conical flow theory is due to the small static margin of the models tested (about $0.025l$). Tests with models having large static margins (such as those generally used in wind-tunnel tests) would obscure this difference and indicate that the static stability of slender cones is more closely predicted by conical flow (or Newtonian) theory.

As in the case of the lift and dynamic stability data for the ablating models (Figs. 7–9), the static stability data with ablation in Fig. 10 also show relatively large scatter, which again is not expected. As stated earlier, this scatter is probably due to varying effects of ablation from flight to flight.

Concluding Remarks

Results of ablation rate calculations have shown the test conditions considered likely to yield aerodynamic data on ablating plastic models in a ballistic range. A series of ballistic range tests of ablating Delrin cones ($\dot m/\rho VA \approx 0.02$) and

¶ Other investigations have shown high sensitivity in the dynamic stability of slender cones depending on test conditions; both large increases[4,5] and large decreases[3,7] in the dynamic stability due to simulated ablation have been noted.

** Results presented in Ref. 3 for a 9° cone coated with paradichlorobenzene show these same two effects, although comparison with either conical flow or Newtonian theory is not made.

†† A similar calculation was made for the model and test conditions of Ref. 3, namely, a 9° half angle cone at $M = 10$, $Re = 0.15 \times 10^6$, and a wall temperature of 300°K. The results showed that the value of $C_{m_{\alpha f}}$ for this case was -0.036, which is again about one-third of the difference between the value of C_{m_α} measured in Ref. 3 for a nonablating model (-0.39) and the value of C_{m_α} predicted by conical flow theory (-0.27).

nonablating metal cones was described. It was found that for the angle-of-attack range investigated, ablation reduced the drag coefficient by about 0.03 (approximately 25% at zero angle of attack), which is in excellent agreement with calculations assuming steady-state ablation. This difference is attributable to a 75% decrease in skin friction due to ablation. It was also found that ablation reduced the static stability by about 35% at angles of attack up to about 10°; calculations indicate that the loss of skin friction accounts for only about one-third of this measured reduction. Conical flow theory (also Newtonian theory) underpredicts the static stability of the nonablating cones by about 35%; hence this estimate is in good agreement with the static stability measured for the ablating cones. The experimental data show further that both the nonablating and ablating models are statically and dynamically stable at the present test coditions and that ablation has little effect on the dynamic stability and lift.

References

[1] Syvertson, C. A. and McDevitt, J. B., "Effects of Mass Addition on the Stability of Slender Cones at Hypersonic Speeds," *AIAA Journal*, Vol. 1, No. 4, April 1963, pp. 939–940.

[2] Syvertson, C. A. and McDevitt, J. B., "Effects of Mass-Transfer Cooling on the Static Stability and Dynamic Motions of Slender Entry Vehicles," *Transactions of the Eighth Symposium on Ballistic Missile and Space Technology*, Vol. III, Air Force Systems Command, San Diego, Calif., Oct. 16–18, 1963.

[3] Chrusciel, G. T. and Chang, S. S., "Effects of Ablation on Hypersonic Aerodynamic Stability Characteristics," AIAA Paper 66-410, Los Angeles, Calif., 1966.

[4] Sacks, I. and Schurmann, E. E., "Aerodynamic Phenomena Associated With Advanced Reentry Systems," RAD-TM-63-79, 1963, Avco Corp., Wilmington, Mass.

[5] Grimes, J. H., Jr. and Casey, J. J., "Influence of Ablation on the Dynamics of Slender Re-entry Configurations," *Journal of Spacecraft and Rockets*, Vol. 2, No. 1, Jan.-Feb. 1965, pp. 106–108.

[6] Ericsson, L. E. and Reding, J. P., "Ablation Effects on Vehicle Dynamics," AIAA Paper 66-51, New York, 1966.

[7] Colosimo, D. D., "Techniques for Aerothermodynamic Testing of Ablating Models in the Wave Superheater Hypersonic Tunnel," AIAA Paper 68-380, San Francisco, Calif., 1968.

[8] Meyers, J. R., "Effects of Symmetrical and Unsymmetrical Mass Addition on the Static-Stability Characteristics of a 7.25-deg. Cone at Mach 8," TR-66-174, 1966, Arnold Engineering Development Center.

[9] Moore, D. R. et al., "Dynamic Stability Wind Tunnel Tests of a 10° Cone With Simulated Ablation at $M = 17$," *AIAA Journal*, Vol. 5, No. 8, Aug. 1967, pp. 1377–1385.

[10] Hube, F. K., "Static Stability Test of an 8-deg. Cone With Ablation at Mach Number 10," TR-65-155, 1965, Arnold Engineering Development Center.

[11] Burt, G. E. and Gregson, J. H., "Effects of Ablation on the Dynamic Stability Characteristics of an 8-deg. Cone at Mach 10," TR-65-92, 1965, Arnold Engineering Development Center.

[12] King, H. H. and Talbot, L., "Effect of Mass Injection on the Drag of a Slender Cone in Hypersonic Flow," *AIAA Journal*, Vol. 2, No. 5, May 1964, pp. 836–844.

[13] Jorgensen, L. H. and Hagen, J. R., "Measured and Computed Static Aerodynamic Characteristics of Ablating Conical Teflon Models at Mach Number 14," TN D-4022, 1967, NASA.

[14] Thyson, N., "Dynamic Stability With Mass Addition—Analysis and Flight Test Comparison," *Transactions of the Second Technical Workshop on Dynamic Stability Testing*, Vol. III, Paper 3, Arnold Engineering Development Center, Air Force Systems Command and ARO Inc., Arnold Air Force Station, Tenn., April 20–22, 1965.

[15] Nelson, A., "Dynamic Stability With Mass Addition—Ground Testing Technique and Results," *Transactions of the Second Technical Workshop on Dynamic Stability Testing*, Vol. III, Paper 4, Arnold Engineering Development Center, Air Force Systems Command, and ARO Inc., Arnold Air Force Station, Tenn., April 20–22, 1965.

[16] Holdhusen, J. S., Casey, J. J., and Decoursin, D. G., "Description of a Phased Blowing Rig for Hypersonic Stability and Some Preliminary Results," *Transactions of the Second Technical Workshop on Dynamic Stability Testing*, Vol. III, Paper 5, Arnold Engineering Development Center, Air Force Systems Command, and ARO Inc., Arnold Air Force Station, Tenn., April 20–22, 1965.

[17] Roberts, M. L. and Cline, P. B., "Simulation and Analysis of the Effect on Dynamic Stability of Mass Addition From a Charring Ablator," *Transactions of the Second Technical Workshop on Dynamic Stability Testing*, Vol. III, Paper 6, Arnold Engineering Development Center, Air Force Systems Command, and ARO Inc., Arnold Air Force Station, Tenn., April 20–22, 1965.

[18] Intrieri, P. F., Kirk, D. B., and Terry, J. E., "Ablation Testing in Ballistic Ranges," AIAA Paper 68-385, San Francisco, Calif., 1968.

[19] Curtis, J. S., "An Accelerated Reservoir Light-Gas Gun," TN D-1144, 1962, NASA.

[20] Malcolm, G. N. and Chapman, G. T., "A Computer Program for Systematically Analyzing Free-Flight Data to Determine the Aerodynamics of Axisymmetric Bodies," TN D-4766, 1968, NASA.

[21] Seiff, A., "A New Method for Computing Drag Coefficients From Ballistic Range Data," *Journal of the Aerospace Sciences*, Vol. 25, No. 2, Feb. 1958, pp. 133–134.

[22] Seiff, A. and Wilkins, M. E., "Experimental Investigation of a Hypersonic Glider Configuration at a Mach Number of 6 and at Full-Scale Reynolds Numbers," TN D-341, 1961, NASA.

[23] Nicolaides, J. D., "On the Free-Flight Motion of Missiles Having Slight Configurational Asymmetries," Rept. 858, 1953, Ballistic Research Labs., Aberdeen Proving Ground, Md.

[24] Seiff, A., Sommer, S. C., and Canning, T. N., "Some Experiments at High Supersonic Speeds on the Aerodynamic and Boundary-Layer Transition Characteristics of High-Drag Bodies of Revolution," RM A56I05, 1957, NASA.

[25] Allen, H. J., "Motion of a Ballistic Missile Angularly Misaligned With the Flight Path Upon Entering the Atmosphere, and Its Effect Upon Aerodynamic Heating, Aerodynamic Loads, and Miss Distance," TN 4048, 1957, NASA.

[26] Chapman, G. T., "Theoretical Laminar Convective Heat Transfer and Boundary-Layer Characteristics on Cones at Speeds to 24 km/sec," TN D-2463, 1964, NASA.

[27] Winovich, W., Unpublished arc-jet data, 1964, Ames Research Center.

[28] Wilkins, M. E. and Tauber, M. E., "Boundary-Layer Transition on Ablating Cones at Speeds up to 7 km/sec," *AIAA Journal*, Vol. 4, No. 8, Aug. 1966, pp. 1344–1348.

[29] *Materials in Design Engineering—Material Selector Issue*, Vol. 64, No. 5, Reinhold, New York, Oct. 1966.

[30] Wentink, T., Jr., "High-Temperature Behavior of Teflon," Rept. 55, July 1959, Avco-Everett Corp.